MULTIMODAL AI-DRIVEN GLOBAL MAPPING OF ANTHROPOGENIC METHANE EMITTERS

Jiahao Li, Xiaomeng Huang*
Department of Earth System Science
Tsinghua University
Beijing

ABSTRACT

Methane is the second most important driver of climate change, and its mitigation is considered a critical near-term strategy for slowing global warming. Anthropogenic activities constitute the dominant source of methane emissions, a significant portion of which originates from facility-scale point sources. While bottom-up inventories are valuable, they often suffer from spatial and temporal gaps. Top-down methods using remote sensing can effectively complement these limitations. The complex characteristics of different methane emitters pose significant challenges for feature-annotation-based object detection algorithms. Here, we present a novel remote sensing detection framework based on vision-language multimodal AI and introduce a Multi-scale Adaptive Sliding Window (MASW) strategy for global-scale identification of anthropogenic methane emitters. Applying this approach globally to satellite imagery, we construct a top-down global inventory comprising 51,076 precisely geolocated facilities across all major emission categories, which far exceeding the coverage of existing bottom-up inventory. We further analyze the spatial distribution of these sources and reveal distinct, development-stage-dependent patterns in emission profiles across economies, thereby elucidating the fundamental distribution patterns of global methane emitters. This inventory and its derived insights provide a critical evidence base for targeted monitoring, verification, and mitigation efforts, supporting the implementation of global climate goals.

1 INTRODUCTION

Methane is the second largest driver of climate change after carbon dioxide, contributing roughly one-third of total warmingEtminan et al. (2016), and it also degrades air quality via tropospheric ozoneZhang et al. (2017). Rapid methane mitigation is therefore a critical near-term pathway for limiting warming to 1.5°CJones et al. (2023); Harmsen et al. (2020). The Global Methane Pledge targets at least a 30% reduction from 2020 levels by 2030Cael & Goodwin (2023); Malley et al. (2023). Yet anthropogenic methane sources—many of them facility-scale point sources—remain poorly characterized and precisely locatedKirschke et al. (2013); Karakurt et al. (2012); Miller et al. (2013); Yusuf et al. (2012), hindering effective governance and mitigationJackson et al. (2020); Chandra et al. (2021). Here, we define an Anthropogenic Methane Emitter as an emission source at the individual facility scale.

Bottom-up inventories remain incomplete and weakly attributed, leaving many facility-scale emitters unmappedOmara et al. (2023); Yang et al. (2024); Jiang et al. (2016). This motivates top-down, remote-sensing-based approaches that can localize emitters at scale and provide actionable geolocation and categorization for monitoring and mitigationSchwietzke et al. (2016); Karakurt et al. (2012). Multimodal vision–language models enable richer scene understanding in remote sensingSun et al. (2022); Yao et al. (2023); Radford et al. (2021); Kirillov et al. (2023); Brown et al. (2025). Leveraging these capabilities, we develop a multimodal AI framework for global tracking of anthropogenic methane emitters and identify 51,076 facility-scale sources with precise geolocation. The inventory spans major sectors, including surface coal mines (4,405), coke plants (862), oil and gas extraction areas (22,209), oil and LNG terminals (1,208), solid waste dumpsites (15,046), and wastewater treatment plants (7,346). Relative to GMET (18,023 facilities), our approach expands the number of localized emitters by 183.4%, providing an actionable basis for source attribution and mitigation.

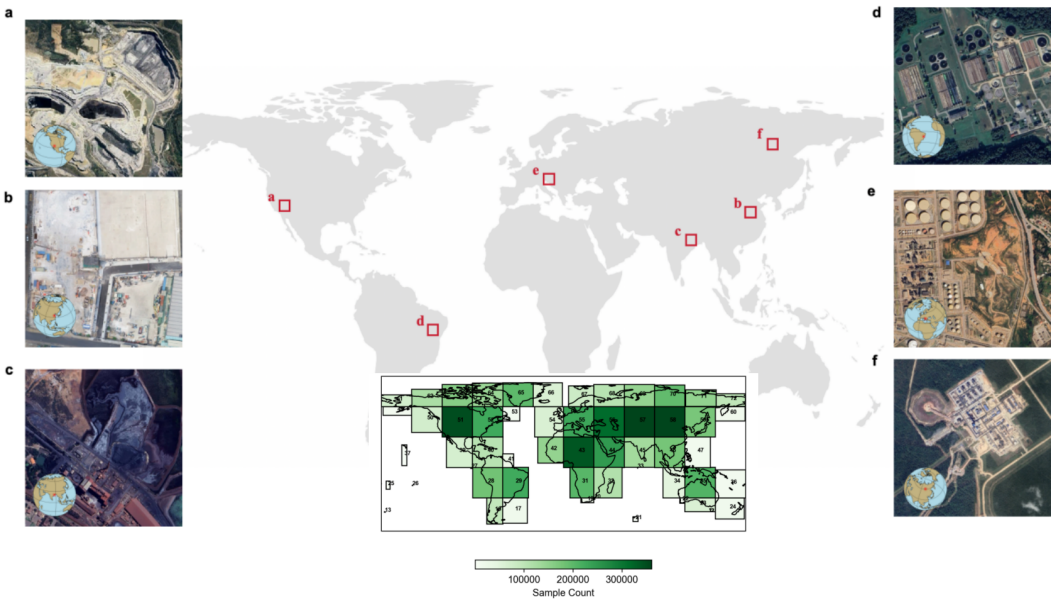

Figure 1: Satellite imagery of major global anthropogenic methane emitters and global distribution of HR remote sensing imagery data a. Surface coal mines; b. Solid waste dumpsites; c. Coke plants; d. Wastewater treatment plants; e. Oil and liquefied natural gas (LNG) terminals; f. Oil and gas extraction areas.

2 METHODS

2.1 DATASET AND GLOBAL TRACKING

We built a global training dataset from high-resolution (HR) remote sensing imageryZhao et al. (2021); Yu & Gong (2012) and used bottom-up inventories to guide annotation and benchmarking. Because Google Earth imagery is mosaicked from multiple sensors (e.g., WorldView/GeoEye), both spatial resolution and revisit frequency vary across regionsGorelick et al. (2017); we therefore assembled a global composite at zoom level 17 (2.15 m), totaling 6,243,816 scenes (Fig.1). We further use the Global Methane Emitters Tracker (GMET; 18,023 facilities) as both an annotation prior and a benchmark for evaluating detection performancede Jong et al. (2025).

2.2 MODEL ARCHITECTURE AND TRAINING DETAILS

Building on the CLIP architecture, we developed a remote sensing image-text alignment model as the core module of our framework (Fig.2). Training samples were manually curated from existing asset-level inventories of anthropogenic methane emitters, ensuring global representativeness across geographic regions. The resulting dataset comprises 5,900 methane-emitting facilities, including 400 coal mines, 800 coke plants, 1,600 oil and gas extraction areas, 600 oil and LNG terminals, 1,500 solid waste dumpsites, and 1,000 wastewater treatment plants. These source categories were selected based on their established significance in the anthropogenic methane emission literature. All samples are derived from zoom level 17 high-resolution remote sensing imagery. During dataset construction, we extracted both the complete facility extent and representative sub-regions, yielding a final set of 18,600 image samples. Each sample was annotated with a structured text prompt following the format category name + detailed description, enabling the model to learn both categorical and fine-grained visual features. Samples with similar visual characteristics shared the same textual description to streamline annotation. We initialized the model using the pre-trained ViT-B-32 weights and fine-tuned it to function as an Image-Text Similarity Computation module within our framework, leading to improved recognition performance on remote sensing imagery of anthropogenic methane emitters. Model training was performed on eight NVIDIA A100 GPUs with an initial learning rate of 1×10^{-4} and a weight decay of 0.1. A linear warm-up schedule was applied

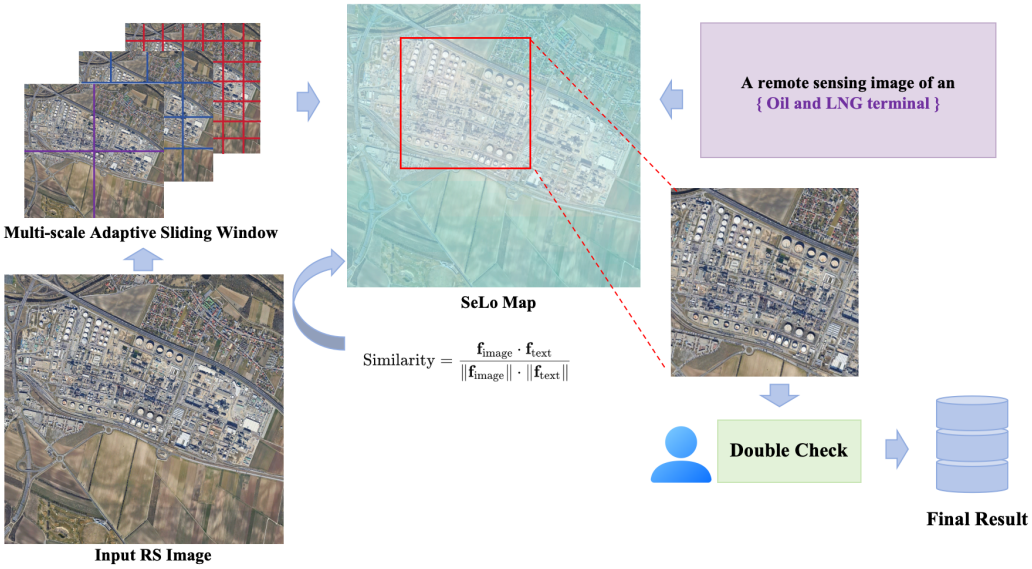

Figure 2: Multi-scale Adaptive Sliding Window (MASW) strategy and detection pipeline.

over the first 10,000 steps to stabilize early training. This configuration supported efficient GPU utilization and stable convergence throughout the optimization process.

Remote sensing images frequently exhibit uneven resolution distribution, a challenge particularly pronounced in regions of anthropogenic methane emitters, where variability in imaging conditions leads to substantial heterogeneity in the size and shape of analogous targets. This complicates detection under a fixed spatial scale.

To address this, we design a detection pipeline that integrates the fine-tuned CLIP model as an image–text similarity computation module and introduces a Multi-scale Adaptive Sliding Window (MASW) strategy (Fig.2). Let I denote the input high-resolution remote sensing image, and let $\mathcal{T} = \{T_k\}_{k=1}^{K}$ be the set of textual prompts describing K categories of anthropogenic methane emitters. A fine-tuned CLIP model, $\mathcal{M}_{\text{CLIP}}(\cdot,\cdot)$, computes a similarity score $s \in [0,1]$ for a given image patch and text prompt.

The MASW performs a hierarchical scan over the entire image using a set of window sizes $\mathcal{W} = \{W_m\}_{m=1}^{M}$ with $W_1 > W_2 > \cdots > W_M$. At each scale m, the image is tiled into a set of patches $\{P_{m,i}\}_{i=1}^{N_m}$ by a sliding window of size $W_m \times W_m$ with stride δ_m. The maximum similarity score for each patch is computed as:

$$s_{m,i} = \max_{T_k \in \mathcal{T}} \mathcal{M}_{\text{CLIP}}(P_{m,i}, T_k). \tag{1}$$

Regions with high similarity scores are identified as high-confidence areas. The framework progressively focuses on these zones to locate concentrated high-score Regions of Interest (ROIs) through a dynamic thresholding scheme. A scale-dependent threshold θ_m is applied, with $\theta_1 < \theta_2 < \cdots < \theta_M$, to enforce progressively stricter confidence requirements. The ROIs at scale m are selected recursively:

$$\text{ROI}_m = \begin{cases} \{P_{1,i} \mid s_{1,i} > \theta_1\}, & m = 1, \\ \{P_{m,j} \mid P_{m,j} \in \mathcal{N}(\text{ROI}_{m-1}),\ s_{m,j} > \theta_m\}, & m \geq 2, \end{cases} \tag{2}$$

where $\mathcal{N}(\text{ROI}_{m-1})$ denotes the spatial neighbourhood around the ROIs obtained at the previous scale. This hierarchical filtering first uses a low threshold during the initial large-window scanning phase to ensure high recall and broadly capture potential ROIs. Within these candidate regions, the window size is progressively reduced while the score threshold is simultaneously raised, enabling finer-scale localization with higher precision.

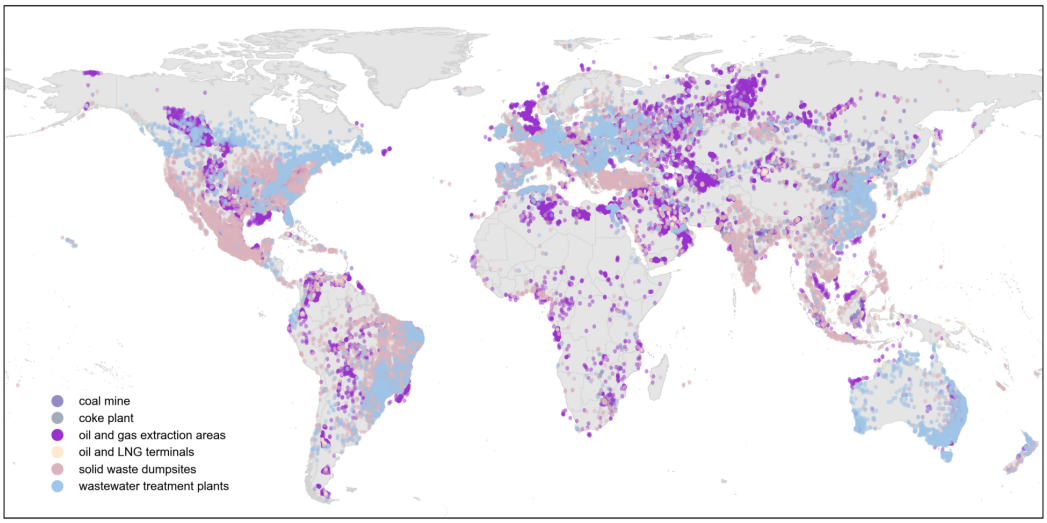

Figure 3: Global map of methane emitters.

After processing the finest scale M, the geographic centroids of the patches in ROI_M form a set of candidate detections:

$$\mathcal{D}_{\text{auto}} = \{\mathbf{loc}_j\}_{j=1}^{J}. \tag{3}$$

Finally, all candidate detections undergo manual verification to confirm their geographic correspondence and classification accuracy, yielding the final validated inventory:

$$\mathcal{D}_{\text{final}} = \{\mathbf{loc} \in \mathcal{D}_{\text{auto}} \mid \mathcal{V}_{\text{human}}(\mathbf{loc}) = \text{True}\}. \tag{4}$$

This hierarchical workflow balances global coverage with local precision, making it suitable for systematic identification of targets across large-area, multi-resolution remote sensing imagery.

3 RESULTS

A global survey using our detection framework yielded a total of 51,076 precisely geolocated anthropogenic methane emission sources, as shown in Fig.3. The inventory spans the full spectrum of major anthropogenic source categories, comprising 4,405 surface coal mines, 862 coke plants, 22,209 oil and gas extraction sites, 1,208 oil and LNG terminals, 15,046 solid waste dumpsites, and 7,346 wastewater treatment plants.

The high-resolution, facility-level inventory fundamentally transforms the paradigm for methane mitigation by enabling a decisive shift from sector-level estimates to facility-level accountabilityKarakurt et al. (2012); Frankenberg et al. (2005); Yusuf et al. (2012),. This granular spatial data moves beyond regional or national averages, allowing regulators, operators, and researchers to attribute emissions to specific industrial assets. Such precision is a prerequisite for implementing transparent monitoring, reporting, and verification (MRV) frameworks, which are essential for carbon markets, regulatory enforcement, and corporate sustainability pledgesJacob et al. (2016); Spahni et al. (2011). For mitigation, the inventory enables a shift from sector-level to facility-level accountability. The precise geolocation of sources allows for direct monitoring of emission trends over time, prioritization of high-density clusters for inspection and repair, and assessment of mitigation policy effectiveness at the sub-national scale. By distinguishing between source types with fundamentally different mitigation pathways, the dataset supports the development of tailored, high-impact reduction strategies. These regionally heterogeneous emission patterns complicate methane governance and highlight the need for spatially explicit inventories. By leveraging multimodal, zero-shot scene understanding, our approach enables scalable tracking of complex remote sensing targets and complements gaps in existing datasets, thereby improving source attribution and emission estimation. This global facility-level inventory provides an evidence base for targeted, cost-effective mitigation to support the Global Methane Pledge and 1.5°C pathways.

REFERENCES

Christopher F Brown, Michal R Kazmierski, Valerie J Pasquarella, William J Rucklidge, Masha Samsikova, Chenhui Zhang, Evan Shelhamer, Estefania Lahera, Olivia Wiles, Simon Ilyushchenko, et al. Alphaearth foundations: An embedding field model for accurate and efficient global mapping from sparse label data. *arXiv preprint arXiv:2507.22291*, 2025.

BB Cael and PA Goodwin. Global methane pledge versus carbon dioxide emission reduction. *Environmental Research Letters*, 18(10):104015, 2023.

Naveen Chandra, Prabir K Patra, Jagat SH Bisht, Akihiko Ito, Taku Umezawa, Nobuko Saigusa, Shinji Morimoto, Shuji Aoki, Greet Janssens-Maenhout, Ryo Fujita, et al. Emissions from the oil and gas sectors, coal mining and ruminant farming drive methane growth over the past three decades. *Journal of the Meteorological Society of Japan. Ser. II*, 99(2):309–337, 2021.

Tobias A de Jong, Joannes D Maasakkers, Itziar Irakulis-Loitxate, Cynthia A Randles, Paul Tol, and Ilse Aben. Daily global methane super-emitter detection and source identification with sub-daily tracking. *Geophysical Research Letters*, 52(8):e2024GL111824, 2025.

Maryam Etminan, Gunnar Myhre, Eleanor J Highwood, and Keith P Shine. Radiative forcing of carbon dioxide, methane, and nitrous oxide: A significant revision of the methane radiative forcing. *Geophysical Research Letters*, 43(24):12–614, 2016.

C Frankenberg, JF Meirink, Michael van Weele, U Platt, and T Wagner. Assessing methane emissions from global space-borne observations. *Science*, 308(5724):1010–1014, 2005.

Noel Gorelick, Matt Hancher, Mike Dixon, Simon Ilyushchenko, David Thau, and Rebecca Moore. Google earth engine: Planetary-scale geospatial analysis for everyone. *Remote sensing of Environment*, 202:18–27, 2017.

Mathijs Harmsen, Detlef P van Vuuren, Benjamin Leon Bodirsky, Jean Chateau, Olivier Durand-Lasserve, Laurent Drouet, Oliver Fricko, Shinichiro Fujimori, David EHJ Gernaat, Tatsuya Hanaoka, et al. The role of methane in future climate strategies: mitigation potentials and climate impacts. *Climatic Change*, 163(3):1409–1425, 2020.

Robert B Jackson, Marielle Saunois, Philippe Bousquet, Josep G Canadell, Benjamin Poulter, Ann R Stavert, Peter Bergamaschi, Y Niwa, Arjo Segers, and Aki Tsuruta. Increasing anthropogenic methane emissions arise equally from agricultural and fossil fuel sources. *Environmental Research Letters*, 15(7):071002, 2020.

Daniel J Jacob, Alexander J Turner, Joannes D Maasakkers, Jianxiong Sheng, Kang Sun, Xiong Liu, Kelly Chance, Ilse Aben, Jason McKeever, and Christian Frankenberg. Satellite observations of atmospheric methane and their value for quantifying methane emissions. *Atmospheric Chemistry and Physics*, 16(22):14371–14396, 2016.

Fei Jiang, Jing M Chen, Lingxi Zhou, Weimin Ju, Huifang Zhang, Toshinobu Machida, Philippe Ciais, Wouter Peters, Hengmao Wang, Baozhang Chen, et al. A comprehensive estimate of recent carbon sinks in china using both top-down and bottom-up approaches. *Scientific Reports*, 6(1): 22130, 2016.

Matthew W Jones, Glen P Peters, Thomas Gasser, Robbie M Andrew, Clemens Schwingshackl, Johannes Gütschow, Richard A Houghton, Pierre Friedlingstein, Julia Pongratz, and Corinne Le Quéré. National contributions to climate change due to historical emissions of carbon dioxide, methane, and nitrous oxide since 1850. *Scientific Data*, 10(1):155, 2023.

Izzet Karakurt, Gokhan Aydin, and Kerim Aydiner. Sources and mitigation of methane emissions by sectors: A critical review. *Renewable energy*, 39(1):40–48, 2012.

Alexander Kirillov, Eric Mintun, Nikhila Ravi, Hanzi Mao, Chloe Rolland, Laura Gustafson, Tete Xiao, Spencer Whitehead, Alexander C Berg, Wan-Yen Lo, et al. Segment anything. In *Proceedings of the IEEE/CVF international conference on computer vision*, pp. 4015–4026, 2023.

Stefanie Kirschke, Philippe Bousquet, Philippe Ciais, Marielle Saunois, Josep G Canadell, Edward J Dlugokencky, Peter Bergamaschi, Daniel Bergmann, Donald R Blake, Lori Bruhwiler, et al. Three decades of global methane sources and sinks. *Nature geoscience*, 6(10):813–823, 2013.

Christopher S Malley, Nathan Borgford-Parnell, Seraphine Haeussling, Ioli C Howard, Elsa N Lefèvre, and Johan CI Kuylenstierna. A roadmap to achieve the global methane pledge. *Environmental Research: Climate*, 2(1):011003, 2023.

Scot M Miller, Steven C Wofsy, Anna M Michalak, Eric A Kort, Arlyn E Andrews, Sebastien C Biraud, Edward J Dlugokencky, Janusz Eluszkiewicz, Marc L Fischer, Greet Janssens-Maenhout, et al. Anthropogenic emissions of methane in the united states. *Proceedings of the National Academy of Sciences*, 110(50):20018–20022, 2013.

Mark Omara, Ritesh Gautam, Madeleine O'Brien, Anthony Himmelberger, Alex Franco, Kelsey Meisenhelder, Grace Hauser, David Lyon, Apisada Chulakadaba, Christopher Miller, et al. Developing a spatially explicit global oil and gas infrastructure database for characterizing methane emission sources at high resolution. *Earth System Science Data Discussions*, 2023:1–35, 2023.

Alec Radford, Jong Wook Kim, Chris Hallacy, Aditya Ramesh, Gabriel Goh, Sandhini Agarwal, Girish Sastry, Amanda Askell, Pamela Mishkin, Jack Clark, et al. Learning transferable visual models from natural language supervision. In *International conference on machine learning*, pp. 8748–8763. PmLR, 2021.

Stefan Schwietzke, Owen A Sherwood, Lori MP Bruhwiler, John B Miller, Giuseppe Etiope, Edward J Dlugokencky, Sylvia Englund Michel, Victoria A Arling, Bruce H Vaughn, James WC White, et al. Upward revision of global fossil fuel methane emissions based on isotope database. *Nature*, 538(7623):88–91, 2016.

Renato Spahni, R Wania, L Neef, M Van Weele, I Pison, Philippe Bousquet, C Frankenberg, PN Foster, Fortunat Joos, IC Prentice, et al. Constraining global methane emissions and uptake by ecosystems. *Biogeosciences*, 8(6):1643–1665, 2011.

Xian Sun, Peijin Wang, Wanxuan Lu, Zicong Zhu, Xiaonan Lu, Qibin He, Junxi Li, Xuee Rong, Zhujun Yang, Hao Chang, et al. Ringmo: A remote sensing foundation model with masked image modeling. *IEEE Transactions on Geoscience and Remote Sensing*, 61:1–22, 2022.

Yuyu Yang, Yongxue Liu, Lei Liu, Zhuqing Liu, and Huansha Wu. Monitoring global cement plants from space. *Remote Sensing of Environment*, 302:113954, 2024.

Fanglong Yao, Wanxuan Lu, Heming Yang, Liangyu Xu, Chenglong Liu, Leiyi Hu, Hongfeng Yu, Nayu Liu, Chubo Deng, Deke Tang, et al. Ringmo-sense: Remote sensing foundation model for spatiotemporal prediction via spatiotemporal evolution disentangling. *IEEE Transactions on Geoscience and Remote Sensing*, 61:1–21, 2023.

Le Yu and Peng Gong. Google earth as a virtual globe tool for earth science applications at the global scale: progress and perspectives. *International Journal of Remote Sensing*, 33(12):3966–3986, 2012.

Rafiu O Yusuf, Zainura Z Noor, Ahmad H Abba, Mohd Ariffin Abu Hassan, and Mohd Fadhil Mohd Din. Methane emission by sectors: a comprehensive review of emission sources and mitigation methods. *Renewable and Sustainable Energy Reviews*, 16(7):5059–5070, 2012.

Zhen Zhang, Niklaus E Zimmermann, Andrea Stenke, Xin Li, Elke L Hodson, Gaofeng Zhu, Chunlin Huang, and Benjamin Poulter. Emerging role of wetland methane emissions in driving 21st century climate change. *Proceedings of the National Academy of Sciences*, 114(36):9647–9652, 2017.

Qiang Zhao, Le Yu, Xuecao Li, Dailiang Peng, Yongguang Zhang, and Peng Gong. Progress and trends in the application of google earth and google earth engine. *Remote Sensing*, 13(18):3778, 2021.